The Pathway by Which the Tetrameric Protein Transthyretin Dissociates†

Ted R. Foss, R. Luke Wiseman, and Jeffery W. Kelly*

Department of Chemistry and The Skaggs Institute of Chemical Biology, The Scripps Research Institute, 10550 North Torrey Pines Road, La Jolla, California 92037

Received August 11, 2005; Revised Manuscript Received September 22, 2005

ABSTRACT: The homotetrameric protein transthyretin (TTR) must undergo rate-limiting dissociation to its constituent monomers in order to enable partial denaturation that allows the process of amyloidogenesis associated with human pathology to ensue. The TTR quaternary structure contains two distinct dimer interfaces, one of which creates the two binding sites for the natural ligand thyroxine. Tetramer dissociation could proceed through three distinct pathways; scission into dimers along either of the two unique quaternary interfaces followed by dimer dissociation represents two possibilities. Alternatively, the tetramer could lose monomers sequentially. To elucidate the TTR dissociation pathway, we employed two different TTR constructs, each featuring covalent attachment of proximal subunits. We demonstrate that tethering the A and B subunits of TTR with a disulfide bond (as well as the symmetrically disposed C and D subunits) allows urea-mediated dissociation of the resulting $(TTR\text{-}S\text{-}S\text{-}TTR)_2$ construct, affording $(TTR\text{-}S\text{-}S\text{-}TTR)_1$ retaining a stable 16-stranded β-sheet structure that is equivalent to the dimer not possessing a thyroid binding site. In contrast, linking the A and C subunits employing a peptide tether $(TTR\text{-}L\text{-}TTR)_2$ affords a kinetically stable quaternary structure that does not dissociate or denature in urea. Both tethered constructs and wild-type TTR exhibit analogous stability based on guanidine hydrochloride denaturation curves. The latter denaturant can denature the tetramer, unlike urea, which can only denature monomeric TTR; hence urea requires dissociation to monomers to function. Under native conditions, the $(TTR\text{-}S\text{-}S\text{-}TTR)_2$ construct is able to dissociate and incorporate subunits from labeled WT TTR homotetramers at a rate equivalent to that exhibited by WT TTR. In contrast, the $(TTR\text{-}L\text{-}TTR)_2$ construct is unable to exchange any subunits, even after 180 h. All of the data presented herein and elsewhere demonstrate that the pathway of TTR tetramer dissociation occurs by scission of the tetramer along the crystallographic C_2 axis affording AB and CD dimers that rapidly dissociate into monomers. Determination of the mechanism of dissociation provides an explanation for why small molecules that bind at the AB/CD dimer−dimer interface impose kinetic stabilization upon TTR and disease-associated variants thereof.

Transthyretin (TTR)[1] is a 127-residue homotetrameric β-sheet-rich protein responsible for the transport of the thyroid hormone, thyroxine, and holoretinol-binding protein in serum and cerebrospinal fluid. Under denaturing conditions, and much more slowly under physiological conditions, TTR is able to dissociate and partially misfold, allowing the process of amyloidogenesis to commence, resulting in a variety of aggregated morphologies including amyloid fibrils (*1*−*8*). This process is associated with three gain of toxic function diseases, familial amyloid polyneuropathy (FAP), familial amyloid cardiomyopathy (FAC), and senile systemic amyloidosis (SSA) (*9*−*11*). The familial forms of these diseases are caused by aggregation of 1 of over 100 energetically destabilized point mutations of TTR, while misfolding and misassembly of the wild-type protein causes the sporadic disease, SSA (*9*−*11*). TTR amyloid deposition occurs in the peripheral nerves, cardiac tissue, the GI tract, and the CNS, the tissue selectivity being partially dictated by the mutation expressed in the patient (*11*, *12*).

The structure of TTR has been characterized extensively by both X-ray crystallography and NMR, demonstrating a dimer of dimers quaternary structure (Figure 1) (*13*−*19*). The asymmetric unit of $P2_12_12$ TTR crystals contains one AB dimer which includes two eight-stranded β-sheets (Figure 1A). The edge to edge β-sheet interface between the A and B subunits represents one quaternary structural interface. Two of these dimers (an AB dimer and the C_2 symmetrically related CD dimer) pack together along their DAGH β-sheet faces forming the second quaternary interface and producing the tetrameric form of TTR and the thyroxine binding sites (Figure 1B,C).

† This work was supported by a grant from the National Institutes of Health (DK46335) and by The Skaggs Institute of Chemical Biology and the Lita Annenberg Hazen Foundation. A graduate fellowship to T.R.F. from Mr. and Mrs. David and Ursula Fairchild is gratefully acknowledged.

* To whom correspondence should be addressed. Phone: (858) 784-9880. Fax: (858) 784-9610. E-mail: jkelly@scripps.edu.

[1] Abbreviations: TTR, transthyretin; TTR-S-S-TTR, disulfide-bonded E92C/C10A mutant TTR construct; TTR-SH, reduced E92C/C10A mutant; TTR-L-TTR, covalently tethered TTR construct; FAP, familial amyloid polyneuropathy; FAC, familial amyloid cardiomyopathy; SSA, senile systemic amyloidosis; GI, gastrointestinal; CNS, central nervous system; FT, Flag tag; GdnHCl, guanidine hydrochloride; CD, circular dichroism; LC-ESI/MS, liquid chromatography/electrospray injection mass spectrometry; HPLC, high-pressure liquid chromatography; TFA, trifluoroacetic acid; SDS−PAGE, sodium dodecyl sulfate−polyacrylamide gel electrophoresis; PMT, photomultiplier tube.

10.1021/bi051608t CCC: $30.25
Published on Web 11/05/2005

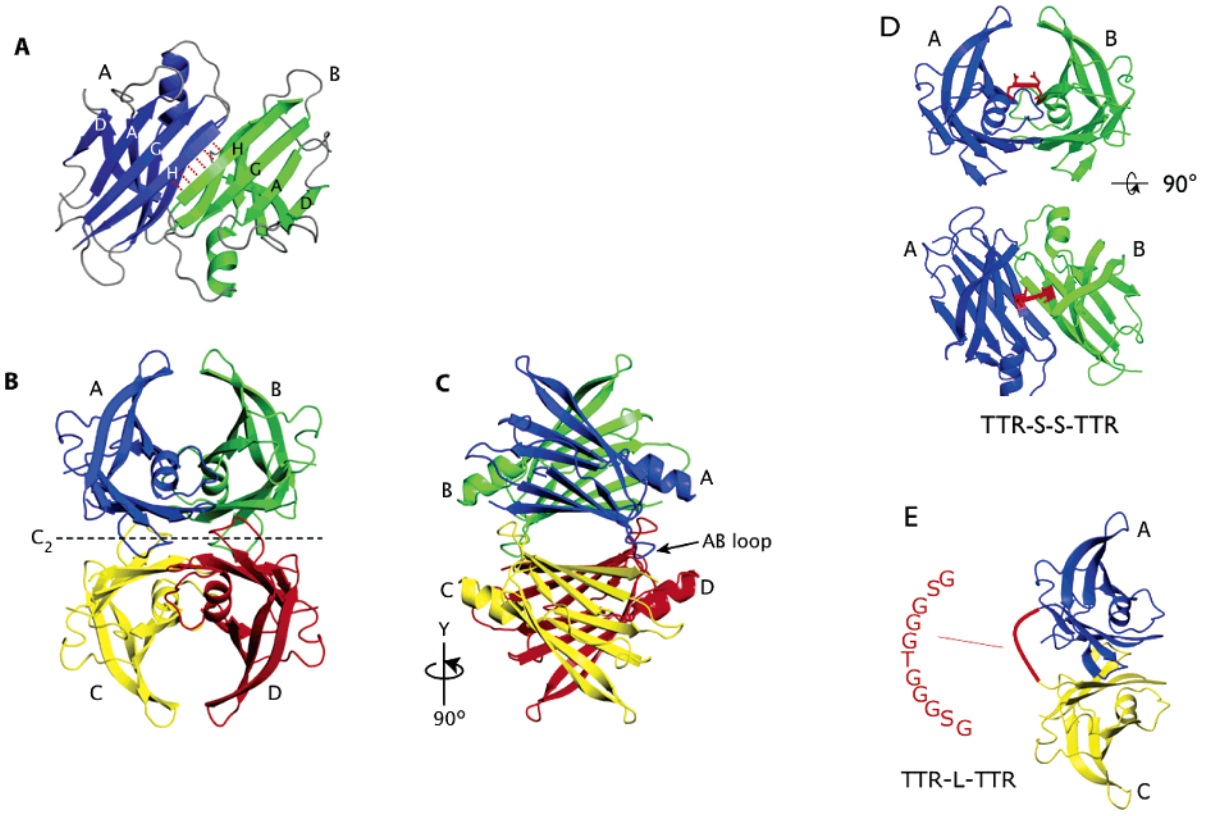

FIGURE 1: Structures of TTR and the tethered constructs. (A) Ribbon diagram of a wild-type TTR AB dimer with the β-strands labeled. Red dashes denote the hydrogen-bonding interface between the H-strands of A and B subunits. (B) Ribbon diagram of tetrameric TTR with each monomer colored differently (subunit A, blue; subunit B, green; subunit C, yellow; subunit D, red). The dotted line represents the crystallographic C_2 axis of symmetry about which a 180° rotation will convert an AB dimer into a CD dimer. (C) Tetrameric TTR rotated 90° about the *y*-axis [relative to the view in (B)] to display the central channel where thyroxine and other ligands bind. (D) Ribbon diagram of TTR-S-S-TTR (subunit A linked to subunit B) showing the location of the Glu-92 residue (red stick figure) that is mutated to Cys to afford a disulfide bond (location denoted by red line). The second view is rotated 90° about the C_2 axis of symmetry as denoted in (B). (E) Ribbon diagram of TTR-L-TTR (subunit A linked to subunit C) denoting the termini linked by the covalent tether, a possible path of the peptide linker (red line), with the amino acid sequence used for the covalent linkage noted.

Tetrameric TTR must undergo rate-limiting dissociation prior to misfolding and amyloidogenesis (*1*, *3*). Whether the fibrils or the smaller soluble aggregates that precede fibrils are the toxic species that mediate pathology is still unclear. Recent results suggest that early amorphous aggregates play an important role (*5*, *20*−*23*). Regardless of which species leads to pathology, prevention of rate-limiting dissociation is the preferred strategy for intervention, as it prevents the entire process of amyloidogenesis from commencing (*24*). Stabilization of TTR by a wide variety of small molecules has been documented, offering promise of TTR amyloidosis treatment by a small molecule drug capable of kinetic native state stabilization (*25*−*33*). Dissociation and aggregation of TTR occur extremely slowly under physiological conditions, while denaturation stresses such as acidic partial denaturation dramatically increase the rate, allowing for observation of amyloidogenesis on a laboratory time scale (*1*, *5*, *20*).

There is typically significant allosteric communication between the two identical thyroxine binding sites giving rise to cooperative ligand binding (*33*−*35*). Negative binding cooperativity is most commonly observed, although noncooperative and positively cooperative small molecules have also been identified (*35*, *36*). We have recently established that binding of a ligand to only one of the two thyroxine binding sites is able to prevent dissociation of the entire quaternary structure, thus preventing amyloidogenesis by selective stabilization of the tetrameric ground state over the dissociative transition state (*18*, *33*, *34*).

There are at least three possible pathways that could enable the tetramer to dissociate leading to monomers (Figure 2); the first two proceed through distinct dimer intermediates. Scission of the tetramer should proceed by dissociation about the energetically weaker dimer interface followed by dissociation of the two resultant dimers (either AB/CD or AC/BD dimers) into monomers. The third possibility, which encompasses three variations, is a monomer loss pathway that proceeds through a trimer and any of three distinct dimers (Figure 2, mechanism 3) on the way to a monomer.

This investigation utilizes two different TTR constructs featuring covalent attachment of proximal subunits to discern which quaternary structural interface is weakest and, thus, which interface will likely come apart first in the process of transthyretin dissociation. One construct $(TTR\text{-}S\text{-}S\text{-}TTR)_2$ is characterized by a cross-link between the A and B subunits (and the symmetry-equivalent C and D subunits), mediated by an engineered disulfide bond between adjacent F−F′ β-strands (Figure 1D). The other $(TTR\text{-}L\text{-}TTR)_2$ construct, previously described (*18*), features a peptide linker that covalently attaches subunits A and C (and the symmetry-equivalent B and D subunits) across the thyroxine binding site interface (Figure 1E). Analysis of the stability of these two chain TTR quaternary structures under both native and

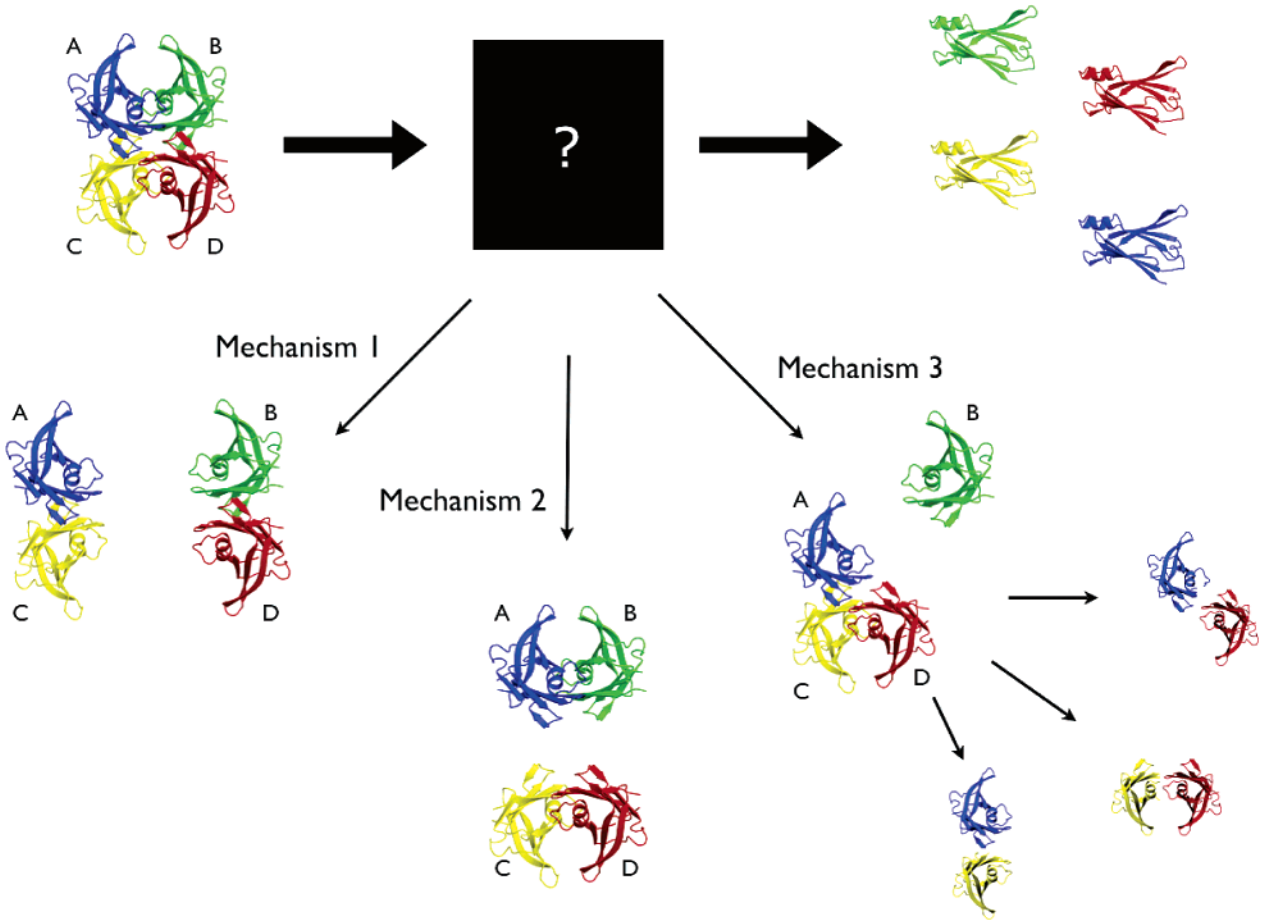

FIGURE 2: Topologically possible dissociation pathways of transthyretin. Subunit labels and color scheme are as in Figure 1B. The tetramer can split along either dimer interface (mechanism 1 or 2), producing two distinct types of dimer intermediates, which can dissociate further affording monomers. Additionally, a single monomer can dissociate from the tetramer to yield a trimer which loses another subunit to produce any of three distinct dimers that then dissociate into their component monomers (mechanism 3).

denaturing conditions offers insight into the initial steps of the pathway by which TTR likely dissociates.

MATERIALS AND METHODS

(TTR-S-S-TTR)$_2$ Design and Purification. Wild-type TTR had two mutations incorporated into the sequence, C10A and E92C. Cys-10 was eliminated to prevent incorrect disulfide bonds from forming, and Glu-92 was chosen for mutation on the basis of its location in strand F such that E92 from one subunit aligns with E92 from the adjacent subunit (Figure 1D). This close proximity was anticipated to allow for disulfide formation without the use of chemical cross-linkers. Both mutations were inserted into the wild-type TTR sequence using QuikChange (Stratagene) protocols. Resultant plasmid was cleaned with a PCR enzyme cleanup kit (Qiagen) and subjected to dideoxy sequencing. Expression and purification were performed as described, with the addition of an I_2 oxidation step prior to the final gel filtration column (*18*). I_2 (1 mM) was added to the TTR fraction pool from the anion-exchange column and was immediately loaded onto the gel filtration column. (TTR-S-S-TTR)$_2$ eluted from the gel filtration column at the same column volume as wild-type TTR. Compound **1** was synthesized as described (*30*).

Structural Properties of TTR-S-S-TTR. Mass spectrometry was performed on an Agilent LC/ESI-MS. Samples were desalted on a 1 mL C_4 column prior to injection into the spray chamber. Quaternary structure determination by gel filtration was performed on an analytical Superdex 75 column attached to an AKTA Explorer FPLC system. Injections of 100 μL of purified proteins were eluted at 0.5 mL/min for 1.2 column volumes. Analytical ultracentrifugation was performed on a Beckman XL-I equipped with an AnTi50 eight-hole rotor. Interference and absorbance optics were used with cells constructed from sapphire windows and 1.2 mm charcoal-filled Epon centerpieces. Samples for velocity experiments were equilibrated at 20 °C for at least 1 h prior to initiation of runs at 50000 rpm for 4 h. Scans were fit using the *c*(*s*) analysis method with the programs SedFit or SedPhat (*37*). Density and viscosity were calculated for all samples utilizing the program Sednterp. HPLC chromatography was performed on a Waters 486 utilizing a gradient of 85% A (95% MilliQ water, 4.9% acetonitrile, 0.1% TFA) and 15% B (4.9% MilliQ water, 95% acetonitrile, plus 0.1% TFA) to 60% B over 10 min.

Chaotrope Stability. TTR, (TTR-L-TTR)$_2$, or (TTR-S-S-TTR)$_2$ (3.6 μM) was incubated in various concentrations of urea or GdnHCl for 96 h at 25 °C. Longer incubations continued at 25 °C, with measurements made at indicated time points up to 330 h. Stocks of urea and guanidine were prepared to 10 M and 7.33 or 8.2 M, respectively, in 10 mM NaP_i, 150 mM KCl, and 1 mM EDTA, pH 7.0, using the index of refraction to verify concentrations. Stability curves were fit as described previously (*18*). Fluorescence

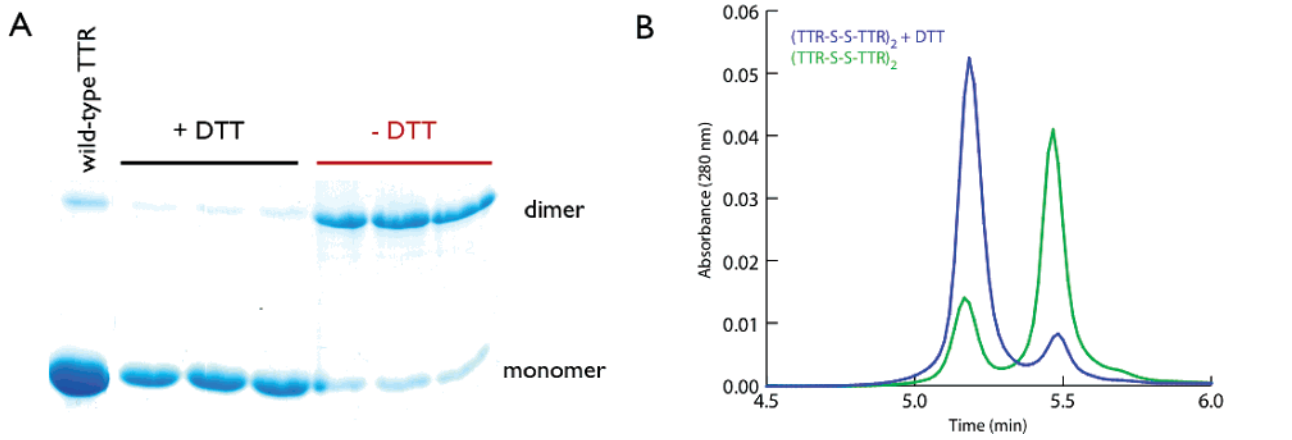

FIGURE 3: $(TTR\text{-}S\text{-}S\text{-}TTR)_2$ construct migrates as a dimer without DTT reduction and as a monomer with reduction. (A) GelCode Blue (Pierce Biotechnologies) stained SDS−PAGE gel displaying $(TTR\text{-}S\text{-}S\text{-}TTR)_2$ bands with and without 1 mM DTT. The three lanes are triplicate repeats of identically treated samples, the wild-type TTR control displaying a dark monomer band, and a light dimer band (wild-type TTR affords SDS-stable dimers after boiling for only 1 min in SDS loading buffer) is shown in the left-most lane. (B) HPLC chromatogram of 1.8 μM $(TTR\text{-}S\text{-}S\text{-}TTR)_2$ in the presence (blue line) or absence (green line) of the reductant DTT. The peak eluting at a retention time of 5.2 min is TTR-SH.

spectra were recorded on a Varian Cary 50 spectrofluorometer with the following parameters: PMT 800 V, fast scan speed, excitation 295 nm, in a 500 μL 1 cm fluorescence cuvette. Six individual scans were averaged together, and the Trp fluorescence emission intensity ratio (defined as the ratio of the tryptophan emission intensity at 355 nm to the tryptophan emission intensity at 335 nm) was used as a measure of foldedness. CD spectra were measured with an Aviv CD-202 circular dichroism spectrometer, using a 0.1 cm path length CD cuvette, averaging three separate scans from 250 to 208 nm, wavelength step 0.5 nm. The wavelength of greatest signal change (218 nm) was used as the measure of foldedness.

Subunit Exchange. $(FT)_4$ protein was prepared as previously described (*18*). Incubation of 3.6 μM total protein [1.8 μM wild-type TTR, or 1.8 μM $(TTR\text{-}L\text{-}TTR)_2$, or 1.8 μM $(TTR\text{-}S\text{-}S\text{-}TTR)_2$ and 1.8 μM $(FT)_4$] was performed in 1.5 mL Eppendorf tubes incubated at 25 °C. At measurement intervals, a 50 μL aliquot was removed and loaded on a SMART system equipped with a 0.5 mL "Q" anion-exchange column equilibrated in 75% A buffer (25 mM Tris, pH 7.0, 1 mM EDTA) and 25% B buffer (A plus 1 M NaCl). A gradient of 25% to 42% B over 45 min afforded a chromatogram with three or five distinct peaks which were digitally integrated.

RESULTS

Protein Design and Production. Creating the $(TTR\text{-}S\text{-}S\text{-}TTR)_2$ construct requires only two point mutations. The wild-type TTR plasmid was subjected to QuikChange mutagenesis to change Cys-10 to Ala and Glu-97 to Cys. Production and purification of the C10A/E92C double mutant followed the protocol described previously for wild-type TTR (*18*). Preceding the final size exclusion step, the protein was concentrated, briefly oxidized with I_2 (5−10 min), and loaded onto a gel filtration column to remove excess iodine. The oxidized version, $(TTR\text{-}S\text{-}S\text{-}TTR)_2$, exhibited a gel filtration profile and an *s*-value profile by velocity analytical ultracentrifugation identical to wild-type TTR, demonstrating a similar overall structure (data not shown). Covalent tethering of neighboring subunits by a disulfide bond allows its reduction to afford a nontethered tetramer enabling control experiments. SDS−PAGE analysis in the presence of DTT (a disulfide-reducing agent) resulted in a major TTR-SH (>90%) band (TTR-SH will refer to TTR-S-S-TTR protein that has been reduced by DTT) which comigrated with wild-type TTR monomer subunits, while SDS−PAGE performed without reducing agent predominantly displayed a band corresponding to a disulfide-linked dimer of TTR, $(TTR\text{-}S\text{-}S\text{-}TTR)_1$ (Figure 3A), demonstrating that a disulfide bond is tethering two TTR subunits together. Incubation of wild-type TTR with SDS loading buffer at room temperature (not boiled) produces an SDS-stable dimer which comigrates with nonreduced TTR-S-S-TTR (data not shown), further supporting the presence of the intact disulfide bond. LC/ESI-MS of nonreduced $(TTR\text{-}S\text{-}S\text{-}TTR)_2$ affords the correct mass for $(TTR\text{-}S\text{-}S\text{-}TTR)_1$ (27668 Da), while reduced $(TTR\text{-}SH)_4$ exhibits the expected monomer mass (13835 Da). HPLC chromatograms under denaturing conditions of $(TTR\text{-}SH)_4$ and nonreduced $(TTR\text{-}S\text{-}S\text{-}TTR)_2$ protein show distinct peaks, enabling quantification of the proportion of oxidized TTR-S-S-TTR and reduced TTR-SH subunits (Figure 3B). I_2 oxidation generally produces $(TTR\text{-}S\text{-}S\text{-}TTR)_2$ in greater than 90% yield. $(TTR\text{-}L\text{-}TTR)_2$ was produced as described previously (*18*).

Relative Stability of $(TTR\text{-}S\text{-}S\text{-}TTR)_2$ and $(TTR\text{-}L\text{-}TTR)_2$. $(TTR\text{-}S\text{-}S\text{-}TTR)_2$ and $(TTR\text{-}L\text{-}TTR)_2$ were subjected to chaotrope denaturation utilizing both guanidine hydrochloride (GdnHCl, Figure 4A) and urea (Figure 4B). Previous work demonstrates that urea cannot directly denature tetrameric TTR; rather it requires dissociation of the tetramer to monomers for denaturation to ensue (*38*). In contrast, GdnHCl can directly denature the tetramer. The $(TTR\text{-}S\text{-}S\text{-}TTR)_2$ GdnHCl denaturation traces are superimposable with the wild-type and $(TTR\text{-}L\text{-}TTR)_2$ traces (Figure 4A, C_m = 5.1, 5.0, and 5.1 respectively). Furthermore, reduction of the disulfide bond to give $(TTR\text{-}SH)_4$ does not alter the GdnHCl denaturation curve (Figure 4A, red squares). Thus the thermodynamic stability of these various quaternary structures is similar, consistent with their analogous structures.

$(TTR\text{-}L\text{-}TTR)_2$ is not amenable to denaturation by urea (Figure 4B), even upon extended incubation periods up to 2

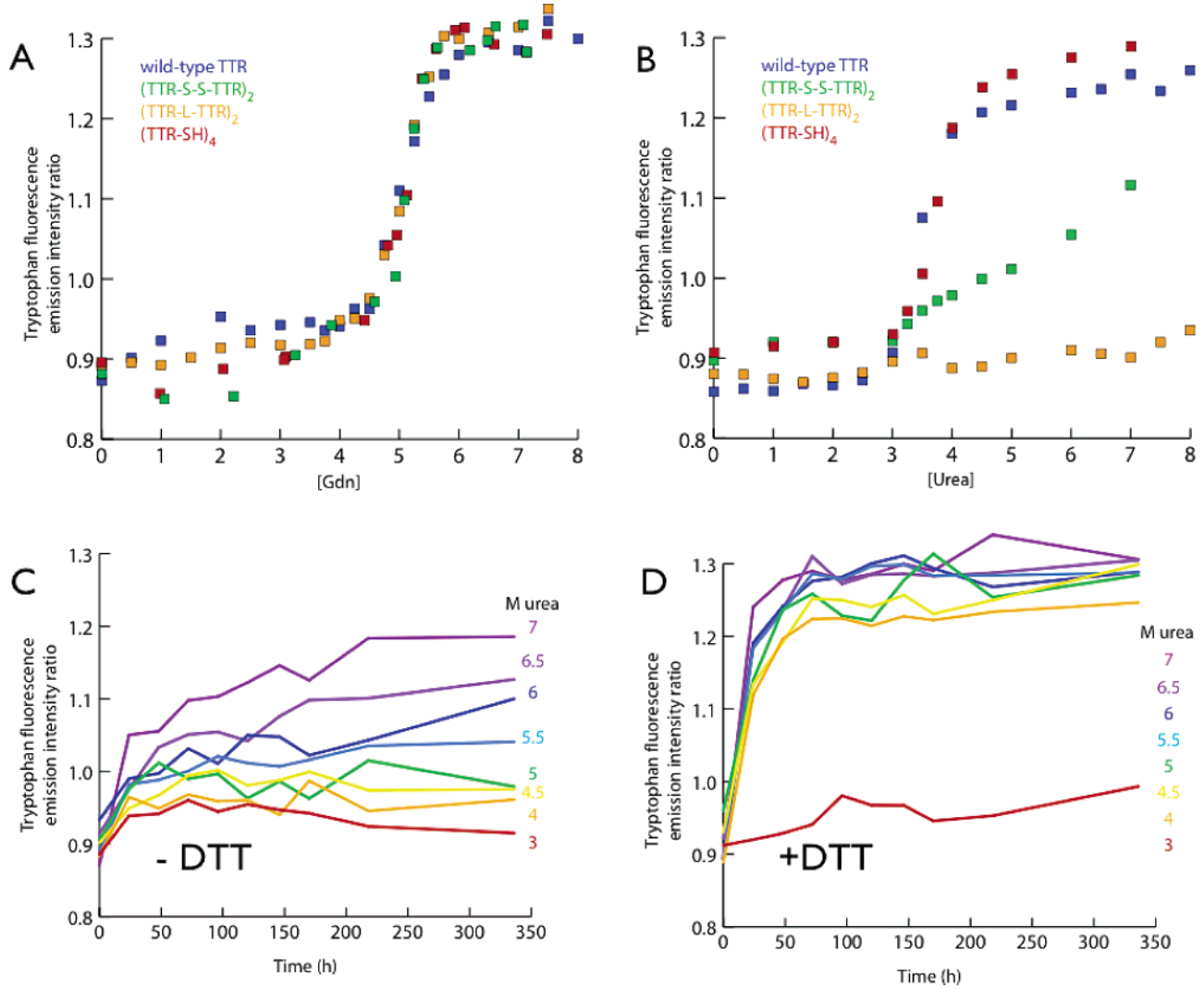

FIGURE 4: (TTR-S-S-TTR)$_2$ and (TTR-L-TTR)$_2$ display distinct susceptibilities to the chaoptropes GdnHCl and urea. GdnHCl (A) and urea (B) stability curves of wild-type TTR (blue), (TTR-S-S-TTR)$_2$ (green), (TTR-L-TTR)$_2$ (orange) (*18*), and (TTR-SH)$_4$ (red). Protein (3.6 μM) was incubated for 96 h at 25 °C at variable chaotrope concentrations prior to measurement of tryptophan fluorescence emission spectra. The tryptophan fluorescence emission intensity ratio displayed is defined as the ratio of the tryptophan emission intensity at 355 nm (unfolded) to the tryptophan emission intensity at 335 nm (folded) and is used as a measure of foldedness. Extended urea denaturation time courses at various urea concentrations utilizing the tryptophan fluorescence intensity ratio to monitor foldedness for (TTR-S-S-TTR)$_2$ in the absence (C) and presence (D) of DTT [affording (TTR-SH)$_4$]. In the absence of DTT, (TTR-S-S-TTR)$_2$ denatures to lesser extent and with slower kinetics compared to samples incubated with DTT, (TTR-SH)$_4$.

weeks, (*18*). Urea denaturation of (TTR-S-S-TTR)$_2$ exhibits significant differences with and without disulfide reductant (Figure 4B). With DTT present, (TTR-SH)$_4$ displays a urea denaturation curve identical to wild-type TTR. In the absence of reductant, (TTR-S-S-TTR)$_2$ appears to be resistant to urea-mediated denaturation when tryptophan fluorescence is used to monitor unfolding. To determine whether the differences in the denaturation traces are due to slow kinetics (slow approach to equilibrium) rather than thermodynamic differences, urea denaturation curves with variable incubation periods were recorded. Extending the urea incubation period of (TTR-S-S-TTR)$_2$ beyond 96 h shows slightly more denaturation, though a wild-type TTR-like denaturation profile is not realized even after 2 weeks of incubation without reductant (Figure 4C). Even at the highest urea concentration employed, 7 M, the tryptophan emission intensity ratio does not reach the plateau level of (TTR-SH)$_4$ (Figure 4D). Far-UV circular dichroism (CD) was employed to monitor denaturation and determine whether the fluorescence-based (TTR-S-S-TTR)$_2$ unfolding curves were recapitulated when monitored by another spectroscopic method that directly assesses β-sheet secondary structure. The resultant CD-based unfolding curves (Figure 5A) overlaid nearly identically with fluorescence-based curves, suggesting that fluorescence unfolding curves were not artifactual. In fact, the far-UV CD spectra as a function of urea concentration exhibit minimal changes, suggesting little loss of β-sheet structure (Figure 5B). Notable CD spectral changes are produced with the DTT-reduced (TTR-SH)$_4$ control (Figure 5C). To further explore the status of (TTR-S-S-TTR)$_2$ in a high concentration of urea (7 M), analytical ultracentrifugation velocity analysis was performed. (TTR-S-S-TTR)$_2$ incubated in 7 M urea exhibited a single monodisperse peak at a sedimentation value of 1.9, consistent with a single disulfide-intact chain, (TTR-S-S-TTR)$_1$, MW = 27 kDa, indicating that dissociation had occurred (Figure 5D). Urea is able to dissociate (TTR-S-S-TTR)$_2$ into (TTR-S-S-TTR)$_1$, but the disulfide-linked AB construct (Figure 1D) is resistant

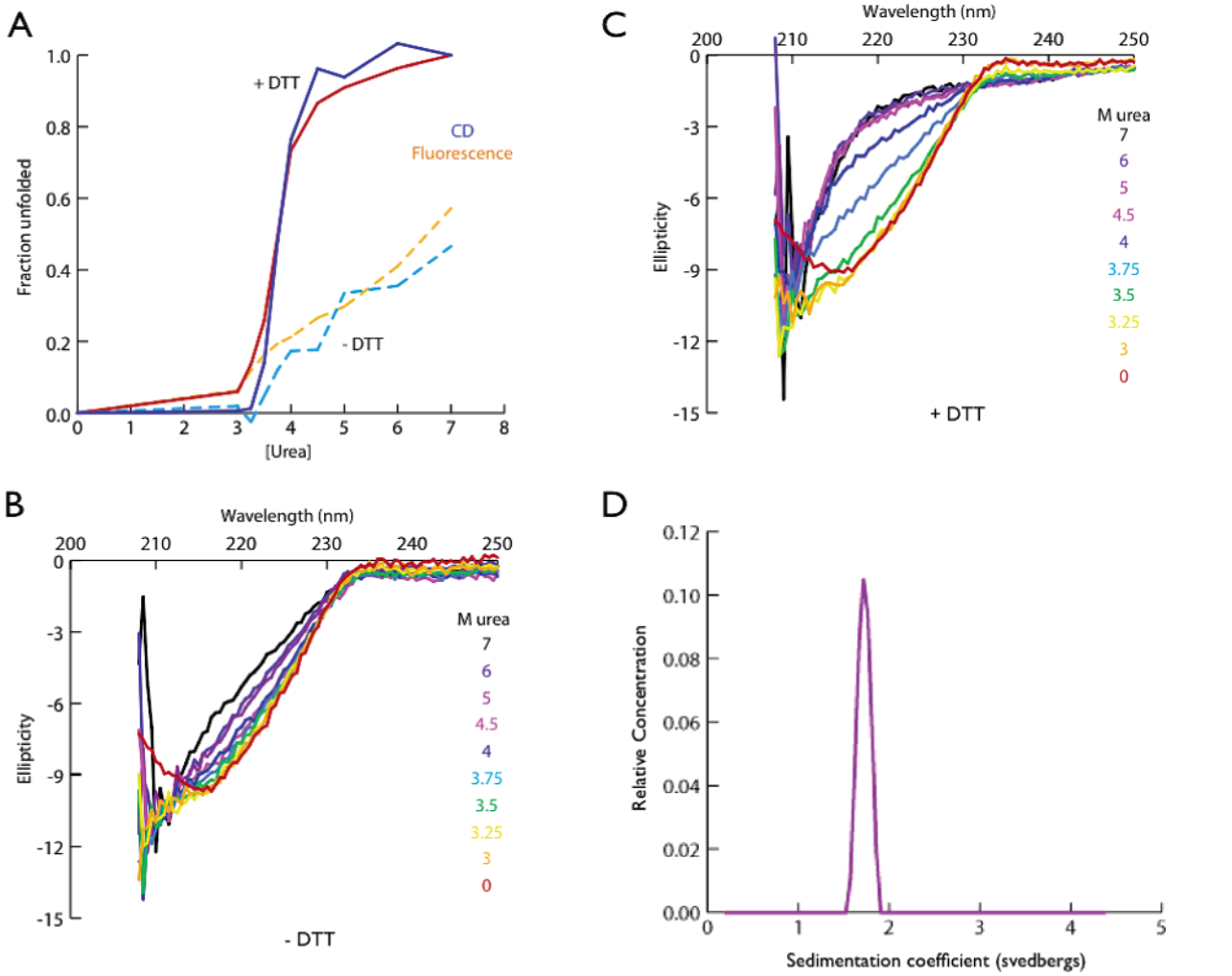

FIGURE 5: $(TTR\text{-}S\text{-}S\text{-}TTR)_1$ tertiary structure is stable to denaturation by urea. (A) Plot of the fraction unfolded $(TTR\text{-}S\text{-}S\text{-}TTR)_2$ (dashed lines) and $(TTR\text{-}SH)_4$ (solid lines) derived from both tryptophan fluorescence [$(TTR\text{-}S\text{-}S\text{-}TTR)_2$, orange dashed; $(TTR\text{-}SH)_4$, red solid] and far-UV CD [$(TTR\text{-}S\text{-}S\text{-}TTR)_2$, light blue dashed; $(TTR\text{-}SH)_4$, dark blue solid] as a function of urea concentration. The fraction unfolded is calculated by dividing the signal at each urea concentration by the signal from the highest urea concentration sample of $(TTR\text{-}SH)_4$. Far-UV CD spectra of $(TTR\text{-}S\text{-}S\text{-}TTR)_2$ (B) or $(TTR\text{-}SH)_4$ (C) at various urea concentrations displaying the conversion from β-sheet secondary structure to a random coil ensemble with increasing urea concentration. Protein (3.6 μM) was incubated at 25 °C for 96 h prior to measurement. (D) Sedimentation velocity $c(s)$ distribution of $(TTR\text{-}S\text{-}S\text{-}TTR)_2$ incubated in 7 M urea for 96 h prior to analysis displaying a single monodisperse peak corresponding to $(TTR\text{-}S\text{-}S\text{-}TTR)_1$ consistent with dissociation but not denaturation as demonstrated in (A) and (B).

to urea denaturation, consistent with both the CD and the fluorescence changes observed. Although the urea denaturation susceptibility of $(TTR\text{-}S\text{-}S\text{-}TTR)_2$ is distinct from that of wild type, the difference is explainable by the kinetic stability of a single 16-stranded $(TTR\text{-}S\text{-}S\text{-}TTR)_1$ β-sheet molecule in urea, further emphasizing the requirement for monomerization in order for TTR to be susceptible to urea denaturation. In other words, a mostly folded AB disulfide-stabilized β-sheet is afforded in urea, consistent with the sedimentation pattern discerned from analytical ultracentrifugation.

Subunit Exchange of $(TTR\text{-}S\text{-}S\text{-}TTR)_2$ and $(TTR\text{-}L\text{-}TTR)_2$. The ability of TTR constructs to dissociate and reassemble under physiological conditions is best ascertained by subunit exchange methodology previously reported by our laboratory (*35*, *39*). A TTR homotetramer composed of monomers with a tandem Flag-tag sequence at their N-termini (homotetramers will be denoted FT_4) is known to dissociate and reassemble with subunits of a wild-type TTR tetramer, affording tetramers with a statistical distribution of subunits as discerned by ion-exchange chromatography. Mixing FT_4 homotetramers with $(TTR\text{-}S\text{-}S\text{-}TTR)_2$ and $(TTR\text{-}L\text{-}TTR)_2$ allows for determination of the extent and rate of dissociation as measured by the formation of the mixed species, $(TTR\text{-}S\text{-}S\text{-}TTR)_1(FT)_2$ and $(TTR\text{-}L\text{-}TTR)_1(FT)_2$, respectively. The appearance of these mixed peaks over time is used to measure the amount of subunit exchange.

The $(TTR\text{-}S\text{-}S\text{-}TTR)_2$ construct is able to exchange with subunits from FT_4 to afford the expected statistical distribution [50% of the total protein present as $(TTR\text{-}S\text{-}S\text{-}TTR)_1FT_2$], over the course of 120 h, with kinetics similar to that of wild-type TTR (Figure 6A). Figure 6B shows a representative chromatogram displaying the peak distribution of $(TTR\text{-}S\text{-}S\text{-}TTR)_2$, $(TTR\text{-}S\text{-}S\text{-}TTR)_1(FT)_2$, and $(FT)_4$. Addition of the potent TTR amyloidogenesis inhibitor **1** (7.2 μM, twice the concentration of TTR and sufficient to occupy both binding sites) is able to prevent subunit exchange from both wild-type TTR and $(TTR\text{-}S\text{-}S\text{-}TTR)_2$, consistent with kinetic stabilization (*35*).

In contrast, the $(TTR\text{-}L\text{-}TTR)_2$ construct does not exhibit any measurable exchange with FT_4 subunits on this or any relevant time scale (measurements made after 9 months of

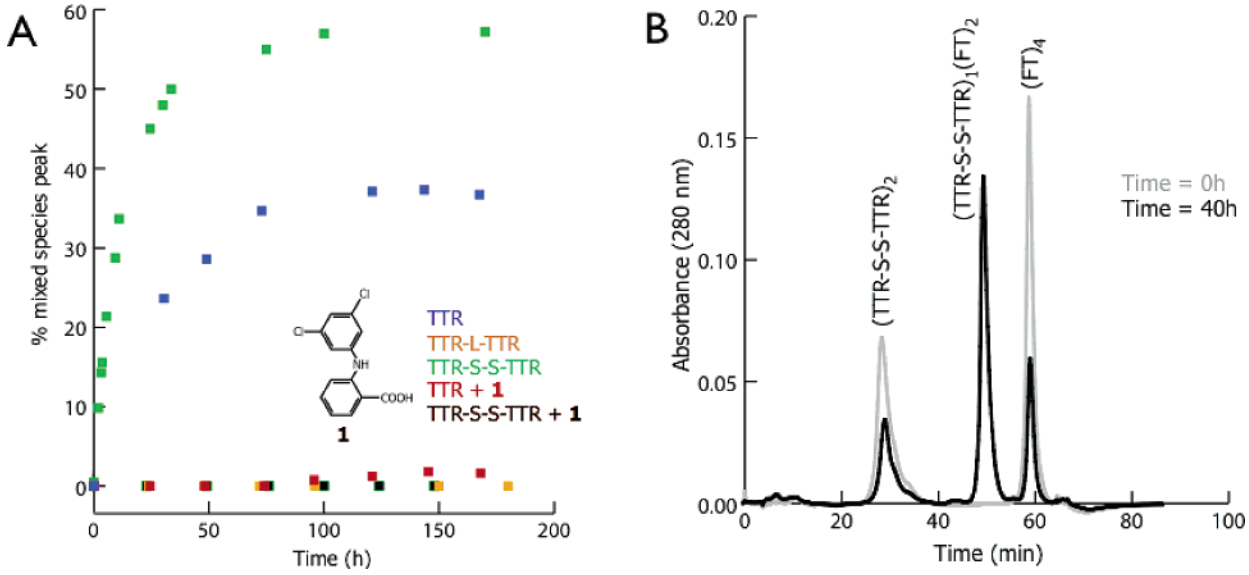

FIGURE 6: Exchange of subunits from $(TTR\text{-}L\text{-}TTR)_2$ and $(TTR\text{-}S\text{-}S\text{-}TTR)_2$ demonstrates dissociation of the latter only. (A) Subunit exchange time course of wild-type TTR, $(TTR\text{-}S\text{-}S\text{-}TTR)_2$, $(TTR\text{-}L\text{-}TTR)_2$, wild-type TTR incubated with the potent amyloidogenesis inhibitor, **1**, and $(TTR\text{-}S\text{-}S\text{-}TTR)_2$ incubated with **1**. Protein (1.8 μM) was incubated with 1.8 μM dual Flag tag TTR homotetramers (FT_4); when present, **1** is at a concentration equal to the thyroxine binding sites present (7.2 μM). Percentage of total protein in the mixed species peak (wild-type $TTR)_2(FT)_2$, $(TTR\text{-}S\text{-}S\text{-}TTR)_1(FT)_2$, or $(TTR\text{-}L\text{-}TTR)_1(FT)_2$ is plotted against incubation time at 25 °C. (B) Representative anion-exchange chromatograms of a $(TTR\text{-}S\text{-}S\text{-}TTR)_2 + (FT)_4$ reaction at incubation times of 0 h (gray) and 40 h (black); the 40 h chromatogram displays three distinct peaks representing $(TTR)_4$, $(TTR\text{-}S\text{-}S\text{-}TTR)_1(FT)_2$, and $(FT)_4$.

incubation show no exchange), consistent with previous results (*18*).

Whereas $(TTR\text{-}S\text{-}S\text{-}TTR)_2$ is able to exchange subunits as rapidly as wild-type TTR, $(TTR\text{-}L\text{-}TTR)_2$ is unable to undergo dissociation and subunit exchange on any biologically relevant time scale. This dramatically distinguishes the two different quaternary interfaces with regard to overall quaternary structural stability under physiologically relevant conditions. Tethering the subunits comprising the AC and BD quaternary interfaces is able to dramatically stabilize the tetrameric structure of TTR. In contrast, stabilization of the AB and CD intermolecular β-sheet interface by disulfide tethering has little discernible effect on quaternary structural stability. Therefore, it appears almost certain that TTR dissociates by mechanism 2 (Figure 2) and that the quaternary structural interface creating the thyroxine binding sites and encompassing the crystallographic C_2 axis (Figure 1B) is the weaker of the two dimer−dimer interfaces in the tetramer. This interpretation is consistent with the urea denaturation data that show that covalent tethering across the AC and symmetry-equivalent BD interfaces prevents dissociation required for urea denaturation, whereas covalent linkage across the AB and symmetry-equivalent CD interfaces does not prevent dissociation of $(TTR\text{-}S\text{-}S\text{-}TTR)_2$ but prevents substantial denaturation because $(TTR\text{-}S\text{-}S\text{-}TTR)_1$ is kinetically stable in urea, owing to its artificial disulfide bond.

DISCUSSION

The $(TTR\text{-}S\text{-}S\text{-}TTR)_2$ and $(TTR\text{-}L\text{-}TTR)_2$ constructs covalently tether the AB/CD and AC/BD quaternary interfaces, respectively. These interfaces were altered in an attempt to identify the weaker of the two interfaces and, thus, the likely pathway of tetramer dissociation. We anticipated that the dimer−dimer interface bisected by the crystallographic C_2 axis is less stable and thus would come apart first (mechanism 2, Figure 2) relative to the other dimer−dimer interface (mechanism 1, Figure 2) based on examination of the crystal structure of wild-type TTR. The AB/CD dimers (Figure 1A) are held together by significant hydrogen-bonding and side-chain−side-chain interactions associated with intermolecular β-sheet interactions between the β-strands (Ser115−Thr123), making dissociation by mechanism 1 unlikely. In contrast, the interface broken in mechanism 2 is stabilized mainly through hydrophobic contacts mediated by the AB and GH loops (Figure 1C) (*17*). Previous work demonstrates that Lys-15 residues located proximal to the crystallographic C_2 axis in the tetramer contribute substantially to quaternary structural stability. These residues have a dramatic destabilizing electrostatic effect on the quaternary interface that dissociates in mechanism 2, a destabilization lessened by increasing ionic strength of the buffer or by mutation to a noncharged residue. For example, the K15A mutation leads to a kinetically stable tetramer (*38*). The stability and dissociation kinetics of $(TTR\text{-}L\text{-}TTR)_2$ and $(TTR\text{-}S\text{-}S\text{-}TTR)_2$ implicate mechanism 2 for dissociation, which is fully consistent with what one would expect from inspection of the structure and from previous data.

That dimer scission (mechanisms 1 and 2) is much more likely than the sequential monomer loss mechanism (mechanism 3) is supported experimentally by previous experiments examining the ability of monomer subunits to dissociate from a $(TTR\text{-}L\text{-}TTR)_1{:}(FT)_2$ molecule (*18*). If mechanism 3 were the main or a contributing pathway of dissociation, incubation of $(TTR\text{-}L\text{-}TTR)_1{:}(FT)_2$ would be expected to equilibrate to the three possible peaks over time. This was not observed; in fact, $(TTR\text{-}L\text{-}TTR)_1{:}(FT)_2$ is kinetically stable for at least 9 months of incubation and does not dissociate, strongly implicating a dimer scission mechanism (*18*).

Further evidence against mechanism 3 for dissociation comes from an analysis of the kinetics of subunit exchange between wild-type TTR and FT_4. Measurement of the

increase or decrease of the concentration of the five different tetramers with distinct subunit stoichiometries as a function of time demonstrates that the rates of formation and disappearance are identical (*35*). That is, each mixed tetramer peak grows at the same rate that the homotetramer peaks decrease. If monomer loss occurred, the 3:1 mixed peaks would be expected to grow much more rapidly than the 2:2 peak, due to the populations of trimer and monomer that result from the dissociation of the first monomer. Equal peak appearance/disappearance kinetics would occur only if dissociation rapidly afforded only monomers which reassemble with a rate that is slow relative to complete dissociation. In order for mechanism 3 to display no bias in peak growth and disappearance kinetics, the second and third dissociation events would have to be much faster; yet, if this were the case, the $(TTR\text{-}L\text{-}TTR)_1$:$(FT)_2$ subunit exchange studies would be expected to display a significant growth of $(TTR\text{-}L\text{-}TTR)_2$ and $(FT)_4$ peaks, which was not observed. These results demonstrate that it is unlikely that TTR dissociates by mechanism 3.

The observation that $(TTR\text{-}S\text{-}S\text{-}TTR)_2$ and wild-type TTR exchange subunits at the same rate strongly supports dissociation by mechanism 2, in contrast to the lack of dissociation observed by $(TTR\text{-}L\text{-}TTR)_2$, ruling out mechanism 1. Mechanism 2, characterized by rate-limiting tetramer dissociation to dimers and then rapid dissociation of the AB and CD dimers to monomers, nicely explains why the five diastereomeric tetramers resulting from exchange of wild-type TTR and FT_4 subunits appear or disappear at the same rates. The fast dissociation of AB and CD dimers is consistent with our inability to detect these intermediates in the course of 10 years of biophysical experiments. Apparently, the AB and CD dimers are not very stable in the absence of additional quaternary interactions, except when disulfide tethered. It therefore stands to reason that TTR should exist in a primarily tetramer−monomer equilibrium, consistent with all of the experimental data collected to date.

The identification of mechanism 2 herein as the TTR dissociation pathway provides insight into kinetic stabilization mediated by small molecule binding to TTR. Binding of various classes of ligands to the thyroxine binding sites of TTR (created by the quaternary structural interface that comes apart first in mechanism 2) has been demonstrated to prevent dissociation and aggregation (*26*, *27*, *31*, *33*, *34*, *40*). X-ray crystallography demonstrates that the binding of a ligand to the thyroxine binding site allows continuous hydrophobic interactions that bridge the A and C subunits (and the symmetry-equivalent B and D subunits) and the carboxylate anion displayed on these compounds attenuates the unfavorable Lys-15−Lys-15′ electrostatic interactions in this interface, further stabilizing the tetramer and preventing dissociation. If scission of either dimer were possible (mechanism 1 or 2), the effects of ligand binding would be to promote dissociation via mechanism 1; yet stable dimers are not detected.

In further support of mechanism 2, stabilization across only one of the two ligand binding sites, through covalent tethering of only the A and C subunits (and not the symmetry-equivalent B and D subunits), is sufficient to kinetically stabilize the entire quaternary structure $(TTR\text{-}L\text{-}TTR)_1(WT)_2$ against dissociation (*18*, *34*). In a similar experiment, we recently tethered a potent inhibitor to one subunit of TTR so that it would only bind to one of the two thyroid hormone binding sites. This singly liganded TTR tetramer is kinetically stable, further supporting mechanism 2. If mechanism 1 was operational, stabilization of one of those dimers should not influence the first dissociation step, which would be expected to produce one stable AC dimer and a BD dimer that could then dissociate into monomers, which was not observed. These results also provide strong evidence against mechanism 3.

Topologically, there are only a limited number of possible dissociation pathways available to a tetrameric protein like TTR. Transthyretin is uniquely suited for a thorough investigation of its dissociation mechanism due to the wealth of previous information about the protein, the capability of engineering distinct, identifiable, tethered subunits, and applicability of techniques that can report on the kinetics and thermodynamics of quaternary interactions. We show that, for TTR, initial dimer scission into AB and CD dimers is followed by rapid dissociation of these dimers to the component monomers. This dissociation pathway of TTR, depicted in Figure 2, mechanism 2, is consistent with all of the experimental results, both herein and previously published, as outlined above. This mechanism of dissociation also nicely rationalizes the kinetic stabilization of TTR imposed by small molecule binding.

REFERENCES

1. Colon, W., and Kelly, J. W. (1992) Partial denaturation of transthyretin is sufficient for amyloid fibril formation in vitro, *Biochemistry 31*, 8654−8660.
2. Hurshman, A. R., White, J. T., Powers, E. T., and Kelly, J. W. (2004) Transthyretin aggregation under partially denaturing conditions is a downhill polymerization, *Biochemistry 43*, 7365−7381.
3. Jiang, X., Smith, C. S., Petrassi, H. M., Hammarstrom, P., White, J. T., Sacchettini, J. C., and Kelly, J. W. (2001) An engineered transthyretin monomer that is nonamyloidogenic, unless it is partially denatured, *Biochemistry 40*, 11442−11452.
4. Kelly, J. W., Colon, W., Lai, Z., Lashuel, H. A., McCulloch, J., McCutchen, S. L., Miroy, G. J., and Peterson, S. A. (1997) Transthyretin quaternary and tertiary structural changes facilitate misassembly into amyloid, *Adv. Protein Chem. 50*, 161−181.
5. Lashuel, H. A., Wurth, C., Woo, L., and Kelly, J. W. (1999) The most pathogenic transthyretin variant, L55P, forms amyloid fibrils under acidic conditions and protofilaments under physiological conditions, *Biochemistry 38*, 13560−13573.
6. Liu, K., Cho, H. S., Lashuel, H. A., Kelly, J. W., and Wemmer, D. E. (2000) A glimpse of a possible amyloidogenic intermediate of transthyretin, *Nat. Struct. Biol. 7*, 754−757.
7. McCutchen, S. L., Colon, W., and Kelly, J. W. (1993) Transthyretin mutation Leu-55-Pro significantly alters tetramer stability and increases amyloidogenicity, *Biochemistry 32*, 12119−12127.
8. McCutchen, S. L., Lai, Z., Miroy, G. J., Kelly, J. W., and Colon, W. (1995) Comparison of lethal and nonlethal transthyretin variants and their relationship to amyloid disease, *Biochemistry 34*, 13527−13536.
9. Westermark, P., Sletten, K., Johansson, B., and Cornwell, G. G., III (1990) Fibril in senile systemic amyloidosis is derived from normal transthyretin, *Proc. Natl. Acad. Sci. U.S.A. 87*, 2843−2845.
10. Connors, L. H., Lim, A., Prokaeva, T., Roskens, V. A., and Costello, C. E. (2003) Tabulation of human transthyretin (TTR) variants, *Amyloid 10*, 160−184.
11. Saraiva, M. J. (1995) Transthyretin mutations in health and disease, *Hum. Mutat. 5*, 191−196.
12. Sekijima, Y., Wiseman, R. L., Matteson, J., Hammarstrom, P., Miller, S. R., Sawkar, A. R., Balch, W. E., and Kelly, J. W. (2005) The biological and chemical basis for tissue-selective amyloid disease, *Cell 121*, 73−85.

13. Blake, C. C., Geisow, M. J., Oatley, S. J., Rerat, B., and Rerat, C. (1978) Structure of prealbumin: secondary, tertiary and quaternary interactions determined by Fourier refinement at 1.8 Å, *J. Mol. Biol. 121*, 339−356.
14. Blake, C. C., Swan, I. D., Rerat, C., Berthou, J., Laurent, A., and Rerat, B. (1971) An X-ray study of the subunit structure of prealbumin, *J. Mol. Biol. 61*, 217−224.
15. Hamilton, J. A., Steinrauf, L. K., Braden, B. C., Liepnieks, J., Benson, M. D., Holmgren, G., Sandgren, O., and Steen, L. (1993) The X-ray crystal structure refinements of normal human transthyretin and the amyloidogenic Val-30→Met variant to 1.7-Å resolution, *J. Biol. Chem. 268*, 2416−2424.
16. Terry, C. J., Damas, A. M., Oliveira, P., Saraiva, M. J., Alves, I. L., Costa, P. P., Matias, P. M., Sakaki, Y., and Blake, C. C. (1993) Structure of Met30 variant of transthyretin and its amyloidogenic implications, *EMBO J. 12*, 735−741.
17. Hornberg, A., Eneqvist, T., Olofsson, A., Lundgren, E., and Sauer-Eriksson, A. E. (2000) A comparative analysis of 23 structures of the amyloidogenic protein transthyretin, *J. Mol. Biol. 302*, 649−669.
18. Foss, T. R., Kelker, M. S., Wiseman, R. L., Wilson, I. A., and Kelly, J. W. (2005) Kinetic stabilization of the native state by protein engineering: implications for inhibition of transthyretin amyloidogenesis, *J. Mol. Biol. 347*, 841−854.
19. Sacchettini, J. C., and Kelly, J. W. (2002) Therapeutic strategies for human amyloid diseases, *Nat. Rev. Drug. Discov. 1*, 267−275.
20. Lashuel, H. A., Lai, Z., and Kelly, J. W. (1998) Characterization of the transthyretin acid denaturation pathways by analytical ultracentrifugation: implications for wild-type, V30M, and L55P amyloid fibril formation, *Biochemistry 37*, 17851−17864.
21. Reixach, N., Deechongkit, S., Jiang, X., Kelly, J. W., and Buxbaum, J. N. (2004) Tissue damage in the amyloidoses: Transthyretin monomers and nonnative oligomers are the major cytotoxic species in tissue culture, *Proc. Natl. Acad. Sci. U.S.A. 101*, 2817−2822.
22. Sousa, M. M., Fernandes, R., Palha, J. A., Taboada, A., Vieira, P., and Saraiva, M. J. (2002) Evidence for early cytotoxic aggregates in transgenic mice for human transthyretin Leu55Pro, *Am. J. Pathol. 161*, 1935−1948.
23. Sousa, M. M., Cardoso, I., Fernandes, R., Guimaraes, A., and Saraiva, M. J. (2001) Deposition of transthyretin in early stages of familial amyloidotic polyneuropathy: evidence for toxicity of nonfibrillar aggregates, *Am. J. Pathol. 159*, 1993−2000.
24. Johnson, S. M., Wiseman, R. L., Sekijima, Y., Green, N. S., Adamski-Werner, S. L., and Kelly, J. W. (2005) Native state kinetic stabilization as a stratgey to ameliorate protein misfolding diseases: A focus on the transthyretin amyloidoses, *Acc. Chem. Res*. (in press).
25. Razavi, H., Palaninathan, S. K., Powers, E. T., Wiseman, R. L., Purkey, H. E., Mohamedmohaideen, N. N., Deechongkit, S., Chiang, K. P., Dendle, M. T., Sacchettini, J. C., and Kelly, J. W. (2003) Benzoxazoles as transthyretin amyloid fibril inhibitors: synthesis, evaluation, and mechanism of action, *Angew. Chem., Int. Ed. Engl. 42*, 2758−2761.
26. Miroy, G. J., Lai, Z., Lashuel, H. A., Peterson, S. A., Strang, C., and Kelly, J. W. (1996) Inhibiting transthyretin amyloid fibril formation via protein stabilization, *Proc. Natl. Acad. Sci. U.S.A. 93*, 15051−15056.
27. Baures, P. W., Oza, V. B., Peterson, S. A., and Kelly, J. W. (1999) Synthesis and evaluation of inhibitors of transthyretin amyloid formation based on the non-steroidal anti-inflammatory drug, flufenamic acid, *Bioorg. Med. Chem. 7*, 1339−1347.
28. Klabunde, T., Petrassi, H. M., Oza, V. B., Raman, P., Kelly, J. W., and Sacchettini, J. C. (2000) Rational design of potent human transthyretin amyloid disease inhibitors, *Nat. Struct. Biol. 7*, 312−321.
29. Oza, V. B., Petrassi, H. M., Purkey, H. E., and Kelly, J. W. (1999) Synthesis and evaluation of anthranilic acid-based transthyretin amyloid fibril inhibitors, *Bioorg. Med. Chem. Lett. 9*, 1−6.
30. Oza, V. B., Smith, C., Raman, P., Koepf, E. K., Lashuel, H. A., Petrassi, H. M., Chiang, K. P., Powers, E. T., Sachettinni, J., and Kelly, J. W. (2002) Synthesis, structure, and activity of diclofenac analogues as transthyretin amyloid fibril formation inhibitors, *J. Med. Chem. 45*, 321−332.
31. Green, N. S., Palaninathan, S. K., Sacchettini, J. C., and Kelly, J. W. (2003) Synthesis and characterization of potent bivalent amyloidosis inhibitors that bind prior to transthyretin tetramerization, *J. Am. Chem. Soc. 125*, 13404−13414.
32. Adamski-Werner, S. L., Palaninathan, S. K., Sacchettini, J. C., and Kelly, J. W. (2004) Diflunisal analogues stabilize the native state of transthyretin. Potent inhibition of amyloidogenesis, *J. Med. Chem. 47*, 355−374.
33. Hammarstrom, P., Wiseman, R. L., Powers, E. T., and Kelly, J. W. (2003) Prevention of transthyretin amyloid disease by changing protein misfolding energetics, *Science 299*, 713−716.
34. Wiseman, R. L., Johnson, S. M., Kelker, M. S., Foss, T., Wilson, I. A., and Kelly, J. W. (2005) Kinetic stabilization of an oligomeric protein by a single ligand binding event, *J. Am. Chem. Soc. 127*, 5540−5551.
35. Wiseman, R. L., Green, N. S., and Kelly, J. W. (2005) Kinetic stabilization of an oligomeric protein under physiological conditions demonstrated by a lack of subunit exchange: Implications for transthyretin amyloidosis, *Biochemistry 44*, 9265−9274.
36. McCammon, M. G., Scott, D. J., Keetch, C. A., Greene, L. H., Purkey, H. E., Petrassi, H. M., Kelly, J. W., and Robinson, C. V. (2002) Screening transthyretin amyloid fibril inhibitors: characterization of novel multiprotein, multiligand complexes by mass spectrometry, *Structure 10*, 851−863.
37. Schuck, P. (2000) Size-distribution analysis of macromolecules by sedimentation velocity ultracentrifugation and lamm equation modeling, *Biophys. J. 78*, 1606−1619.
38. Hammarstrom, P., Jiang, X., Deechongkit, S., and Kelly, J. W. (2001) Anion shielding of electrostatic repulsions in transthyretin modulates stability and amyloidosis: insight into the chaotrope unfolding dichotomy, *Biochemistry 40*, 11453−11459.
39. Schneider, F., Hammarstrom, P., and Kelly, J. W. (2001) Transthyretin slowly exchanges subunits under physiological conditions: A convenient chromatographic method to study subunit exchange in oligomeric proteins, *Protein Sci. 10*, 1606−1613.
40. Peterson, S. A., Klabunde, T., Lashuel, H. A., Purkey, H., Sacchettini, J. C., and Kelly, J. W. (1998) Inhibiting transthyretin conformational changes that lead to amyloid fibril formation, *Proc. Natl. Acad. Sci. U.S.A. 95*, 12956−12960.

BI051608T